

5 Initial Sediment Dispersion Near a Dredged Material Discharge

Fluid-mud thickness, concentration structure, and overlying water-column suspension concentration were measured in shallow Laguna Madre within about 500 m of where a dredge pipeline was discharging. Water depths were 0.5 to 2 m and currents were weak. The dredged material had a median particle size of 4 to 5 μm . Median fluid-mud thicknesses were 0.45 m, of which the top 60 percent was interpreted as underflow and the remainder as deposit. Fluid-mud concentration at the upper surface of the underflow layer was about 3 dry-kg/m³ (3,000 mg/l) and increased exponentially with depth to about 48 dry-kg/m³. The deposit was 48 to 110 dry-kg/m³ solids.

A plume of suspended sediment 200 to 500 mg/l above ambient concentration occurred over the underflow footprint, with resuspension driven by wind-waves. The water column plume was examined only in the proximity of the discharge, and no attempt was made to characterize its entire extent. The development of a point model describing the water column overlying a fluid mud layer was based on a balance between entrainment and settling. Settling was prescribed on the basis of a laboratory-developed functional dependence on concentration. Data were used in the model to estimate coefficients for this entrainment process.

Introduction

Initial dispersion of dredged material after pipeline discharge is important to deposit area and susceptibility to erosion or resuspension. Initial or near-field dispersion is specified in the far-field sediment transport model to be described in the chapters that follow. Observed dispersion near the pipeline discharge consisted of a fluid-mud gravity underflow which formed a deposit and an overlying water-column plume. The fluid-mud gravity flow is a short-lived, initial phase of dispersion lasting perhaps some hours and ending at a down-slope location where the flow stopped. Observations at similar sites suggest that after coming to rest, the underflow continues to deposit and consolidate, with some fraction resuspended and transported away. This latter long-term dispersion is describe in the far-field numerical sediment transport model.

Measurements of fluid-mud thickness, concentration structure, and overlying suspension concentration were made north of Port Mansfield, Texas, in Laguna Madre, within about 500 m of an ongoing dredged-material pipeline discharge. Such information is scarce but is needed to improve understanding of the behavior of such discharges and subsequent sediment dispersion. Information was used to characterize pipeline discharges in a large-scale numerical sediment-transport model of this system described in the next chapter. During and just after initial dispersion, fine, cohesive sediments forming the final deposit are soft and easily resuspended by currents and/or wind-waves. A simple water-column point model was used to estimate coefficients for an entrainment relationship that describes the flux of underflow sediment into the water column. The intent of the point model was to characterize conditions in the vicinity of the underflow and deposit. As will be shown, the extent of the underflow affects the extent of the most highly concentrated surface plume of suspended sediment which might form during or shortly after discharge as a result of entrainment of underflow or deposit into the overlying water column. No attempt will be made here to define the ultimate spatial extent of the surface plume, as those calculations are made in the far-field model of the lagoon.

Pipeline Discharge Underflows

Dredged sediment particles reach the bottom soon after pipeline discharge in shallow water, settling within a short distance from the discharge point. As the bottom layer thickens at the point of discharge, it behaves as a density flow and spreads under the influence of gravity (Neal et al. 1978). Sediments form layers of fluid mud at the bed, which flow away from the point of discharge, the extent of the flow depending on bottom slope, ambient currents, and their initial discharge trajectory. It has been previously estimated that 95 to 99 percent of discharged sediment mass descends to the bottom layers within about 30 m from the point of a pipeline discharge (Schubel et al. 1978; and Neal et al. 1978). In Mobile Bay, for example, 99 percent of the discharged sediment was found to be dispersed along the bottom as fluid mud (Nichols et al. 1978).

The range of concentrations for the fluid-mud definition used here is roughly 5 to 400 dry-kg/m³ (corresponding roughly to 1,003 to 1,250 wet-kg/m³ density). Concentrations of pipeline-discharge solids are within this range, and solids are generally about 15 percent by weight or 150 to 200 dry-kg/m³ (Schubel et al. 1978).

The approach channel to the Chesapeake & Delaware Canal in Upper Chesapeake Bay was hydraulically dredged in 1988. About 5.2×10^5 m³ of clayey-silt sediment were pumped and deposited in Areas D, E, and F near Pooles Island. Depths were 2.5 to 3.5 m before disposal at Area D where most of the material was placed. The movement of sediment was down-slope after discharge. A broad continuous layer formed about 3 km long and 1.5 km wide. The maximum deposit thickness was 1.5 m. Sediment consolidated to a density of 1,130 kg/m³ or greater within several weeks. Dewatering and compaction accounted for 5 percent deposit-volume reduction in 5 months. Another 5 percent reduction occurred during the discharge period. The remaining 22

percent of the 32 percent total reduction was from redistribution by resuspension and transport (Panageotou and Halka 1990).

Near Pooles Island, $5.2 \times 10^5 \text{ m}^3$ of sediment were hydraulically dredged from the nearby channel in 1991 and placed in Areas D and E. Sites were 4.5 to 8 m deep. Sediments deposited in a natural trough and constructed trenches. The sediment remained in the deep, trough area. The volume of the deposit was $1.04 \times 10^6 \text{ m}^3$ with maximum thickness of 3 m. Sediment was clayey silt with minor sand. Bulking factor between in-place and deposited volumes was about 1.75. One year later the deposit was $4.4 \times 10^5 \text{ m}^3$ (58 percent reduction). Four-fifths of the reduction was attributed to dewatering, one-fifth to erosion (Panageotou and Halka 1994).

Underflow spreading controls the configuration of the final deposit. Limited observations indicate that the final deposit is a series of strata laid down as the underflow shifts and grows larger in response to bottom topography. Maximum deposit thickness was about 0.3 m for a typical 2-day disposal operation in Mobile Bay and about 1.8 m for a 10-day disposal in the James River (Nichols et al. 1978).

Field Observations

Field experiments were carried out to take advantage of dredging conducted in February 2000 to remove a 1.8-m layer of material deposited in the GIWW as a result of a hurricane the previous year. *Dredge J.N. Fisher* discharged into open-water disposal sites through a 50.8-cm diam pipeline, using a 1,500-kw (2,000-horsepower) pump. The dredging rate was about $1,100 \text{ m}^3/\text{hr}$, and, based on the solids content of the channel material, the sediment discharge rate was about 50 dry-kg/sec.

Fluid-mud thicknesses, or heights, and densities were measured on two days while pipeline discharge was occurring. Locations for the discharges are shown in Figure 49. A special push-tube sampler allowed for fluid-mud density determination within only a few minutes of sampling. Samples were collected for analysis of the fluid-mud concentration to supplement the field-density measurements. Fluid-mud particle-size distribution and ambient water column suspended-sediment concentrations were also measured. A composite sample was used in the laboratory to determine velocities in the hindered settling range.

Field methods

A 5.8-m-long flat bottomed boat with a propeller tunnel to minimize draft was used for sampling. A Starlink® Differential Global Positioning System was used to locate stations to within $\pm 2 \text{ m}$, and an HP PalmPC® was used to log positions in the field. Water-column samples were collected with a submersible Rule® electric pump and 1.5-cm diam hose. Water samples were collected at mid-depth and 0.3-m depth and stored in 225-ml plastic bottles.

Fluid mud was sampled with a push corer with a clear 3.6-cm diam core tube and a total length of about 3 m. During the first sampling day, it was found that

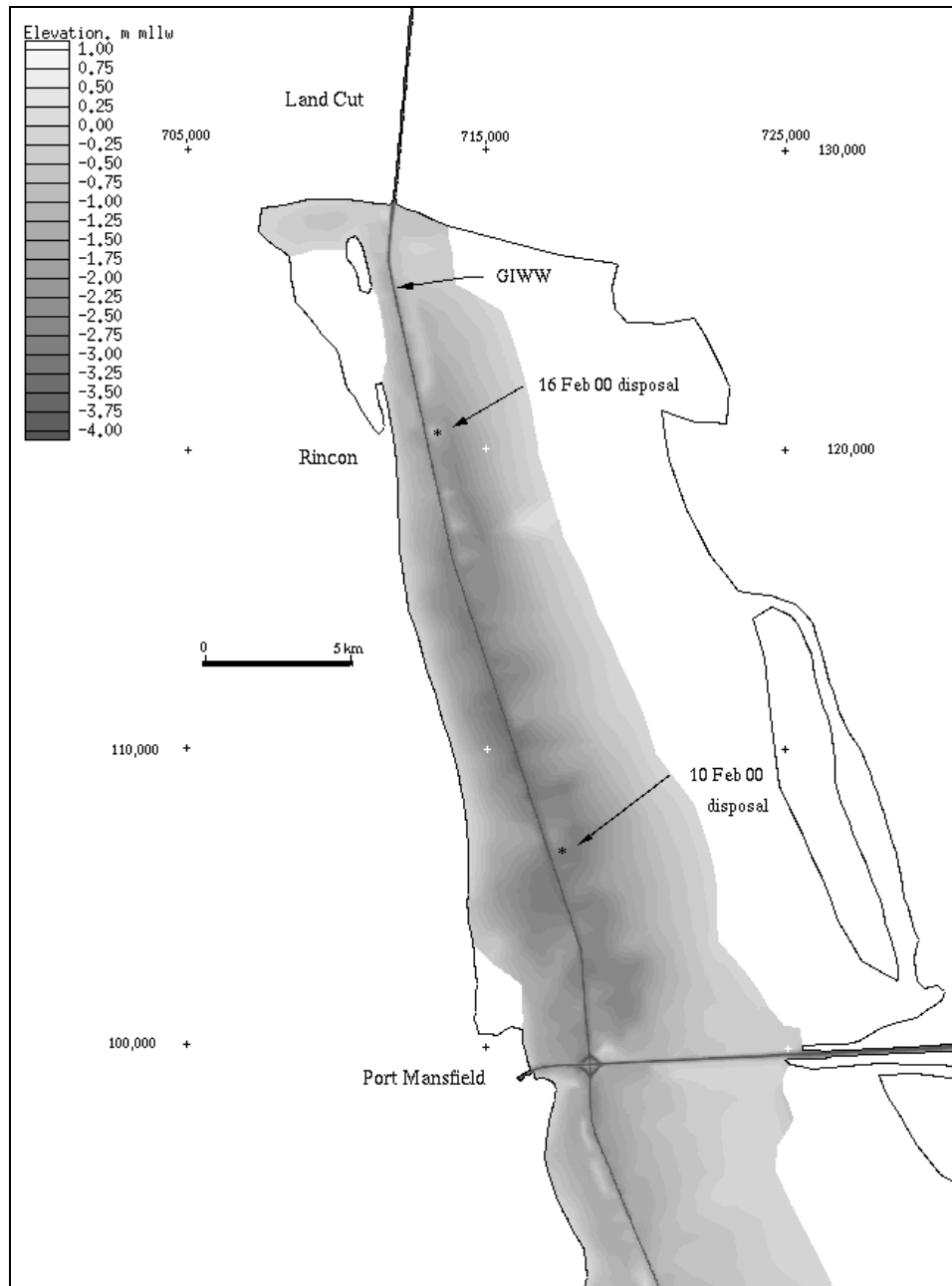


Figure 49. Vicinity sketch of Lower Laguna Madre north of Port Mansfield, Texas, with depth contours and discharge locations (coordinates are state plane NAD27, Texas South, in meters)

the in-line check-valve developed too much back pressure, resulting in significant errors in underflow sampling. For the second sampling day, fluid-mud samples were collected with a low back-pressure push-core sampler specially fabricated from parts of a WILDCO ® corer. That sampler can be seen in Figure 50. Only the fluid-mud measurements from the second day are reported.

The boat was brought to a new location, and the anchor was set. A couple of minutes were allowed for the boat to swing to and for the position to be logged. The corer was pushed vertically downward by hand until it encountered firm bottom. A trip line was then pulled to seal the top of the sampling tube. The corer captured ambient water column, fluid mud (if present), and a short plug of the underlying bottom material. (The bottom material contained an appreciable sand fraction not present in the dredged material and had a bulk density of roughly $1,500 \text{ kg/m}^3$). The vertical alignment of the core tube was maintained as it was lifted to the deck and a piston push-rod was inserted into the lower end of the core tube (below the sediment plug). After the core tube was unscrewed from the remainder of the sampler, the piston rod was pushed upward to expell sample from the end of the tube. By incrementally extruding sample from the end of the core tube, scientists could take measurement and sub-samples over the vertical dimension of the fluid mud. Density measurements were made in the field with a PARR ® DMA35 vibrating-tube densitometer (precision of 1 kg/m^3). A short length of 2-mm diameter tubing was inserted 2.5 cm into the end of the core tube, and a 5 to 10 cm^3 sample was drawn through the densitometer. Field density measurements were made in duplicate and averaged.

Laboratory methods

Laboratory bulk wet density determinations were made with the use of 25-cm^3 wide-mouth pycnometers. Pycnometers were weighed after being mostly filled with sample and then carefully topped with distilled water. Bulk wet density was calculated from this information and known characteristics of the pycnometers. Pore-fluid density was estimated on the basis of the salinity determined on suspended samples, allowing the calculation of sample solids content from bulk wet density (assuming a solids density of $2,650 \text{ kg/m}^3$).

Total suspended material (TSM) was determined by a gravimetric method for non-filterable solids with preweighted Nuclepore ® $0.4 \mu\text{m}$ pore diam, polycarbonate filters. After being used to filter a known volume, filters were rinsed with distilled water and dried one hour at $90 \text{ }^\circ\text{C}$ and then reweighed. Particle-size distribution was measured with a Coulter LS100Q ® laser scattering instrument. Samples were first oxidized with Clorox ® to remove organics and then were dispersed with sodium carbonate/bicarbonate. Three oxidation steps and three dispersion steps were performed before samples were processed through the Coulter instrument to determine particle size. The Coulter has 128 geometrically spaced channels, or bins, for sizing.

Settling velocities in the hindered-settling concentration range were measured on left-over sample that had been composited to make a slurry. The slurry had a bulk density of $1,109.5 \text{ kg/m}^3$, pore-fluid density of $1,025.7 \text{ kg/m}^3$

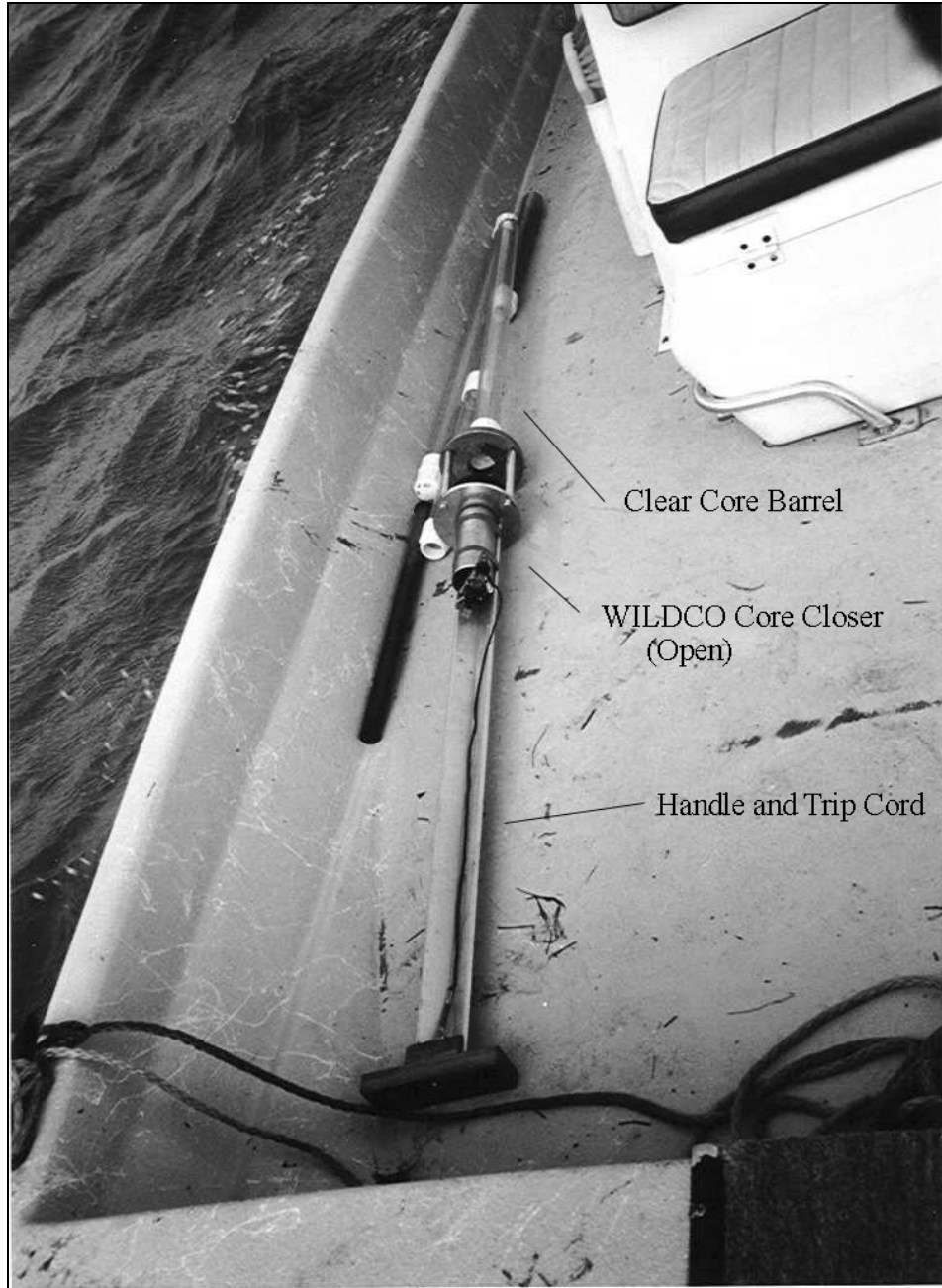


Figure 50. Fluid-mud sampler on deck in the open position

(37.3 ppt salinity), and solids content of 136.7 dry-kg/m³. Sample was incrementally added to a 2 liter glass, graduated cylinder which was 7.74 cm in diam and 42.5-cm high at the 2-liter level. Six tests with concentrations of 6.8 to 66.3 dry-kg/m³ were made at 23 °C. After the sample was mixed in the cylinder, the height of the interface between the suspension and the clear layer that formed was observed over time. The duration of the lowest initial-concentration test was about an hour. During other tests, frequent measurements were collected over 100 to 240 min; these tests lasted a total of 1,100 to 1,450 min. Final data points allowed for estimation of average density after about one day of settling time.

Linear regressions were fit to the data for the period when the interface descended linearly ($n = 3$ to 20, $R^2 = 0.944$ to 0.999, standard error on slope = 1.82 to 0.025 mm/min) to determine the hindered settling velocity (W_s) at initial test concentration C . Tests with the lowest two concentrations were repeated, and data sets were combined in the regression analysis. Finally, W_s and initial concentration from the six tests were combined and fit to an empirical equation for hindered settling dependence on concentration

$$W_s = Wh_o (1 - kC)^n, \quad C > \text{hindered-settling threshold} \quad (38)$$

where the hindered settling threshold is usually in the range of 1 to 10 dry-kg/m³.

Field and laboratory results

All settling tests were in the hindered settling concentration range. Settling rates decreased about two orders of magnitude over the concentration range tested. Data greater than 6.8 dry-kg/m³ fit Equation 1 well with the reference hindered settling velocity $Wh_o = 0.5$ mm/sec, coefficient $k = 0.005$ m³/kg, and the exponent $n = 11$. Settling test results are plotted in Figure 51 along with results from the low-concentration settling tests performed by Teeter et al. (2001a), using Laguna Madre GIWW sediments collected about 3 km north of Port Isabel. The mean depth-average concentration at the end of the settling tests (about 20 hrs) was 115.5 dry-kg/m³ (with one high outlier of 148 dry-kg/m³ removed, $n = 4$, 95 percent confidence interval 112.0 to 118.9 dry-kg/m³).

February 10. When sampling began at 1000 Central Standard Time (CST) on 10 February, south winds were 9 m/sec, making sampling conditions very difficult. Currents were weak and toward the south. The pipeline discharge was located at coordinates 26° 37.4358' N and 97° 24.8643' W, about 3.7 km north of the entrance to Port Mansfield at the disposal area designated PA 218. See Figure 49. The end of the pipe discharged horizontally about 0.6 m above the water surface. A plot of the station locations, CST and depths in a local horizontal coordinate system are shown in Figure 52. The origin for the local coordinate system is at state plane 106,000 m N and 717,000 m E (NAD27, Texas South). The pipeline was located 20 m west of the 1016 CST station and changed only slightly as the dredge moved. Water-column samples taken at 0.3 m depth had TSM levels (mean = 211 mg/l, 95 percent confidence interval 51 to 370 mg/l, $n = 12$) equivalent to those from mid-depth (mean = 199 mg/l, 95 percent confidence interval 55 to 344 mg/l, $n = 11$). Both sampling depths showed highly variable TSM. Depth averaged TSM are shown in Figure 53. High TSM values were measured both north and south of the pipeline discharge.

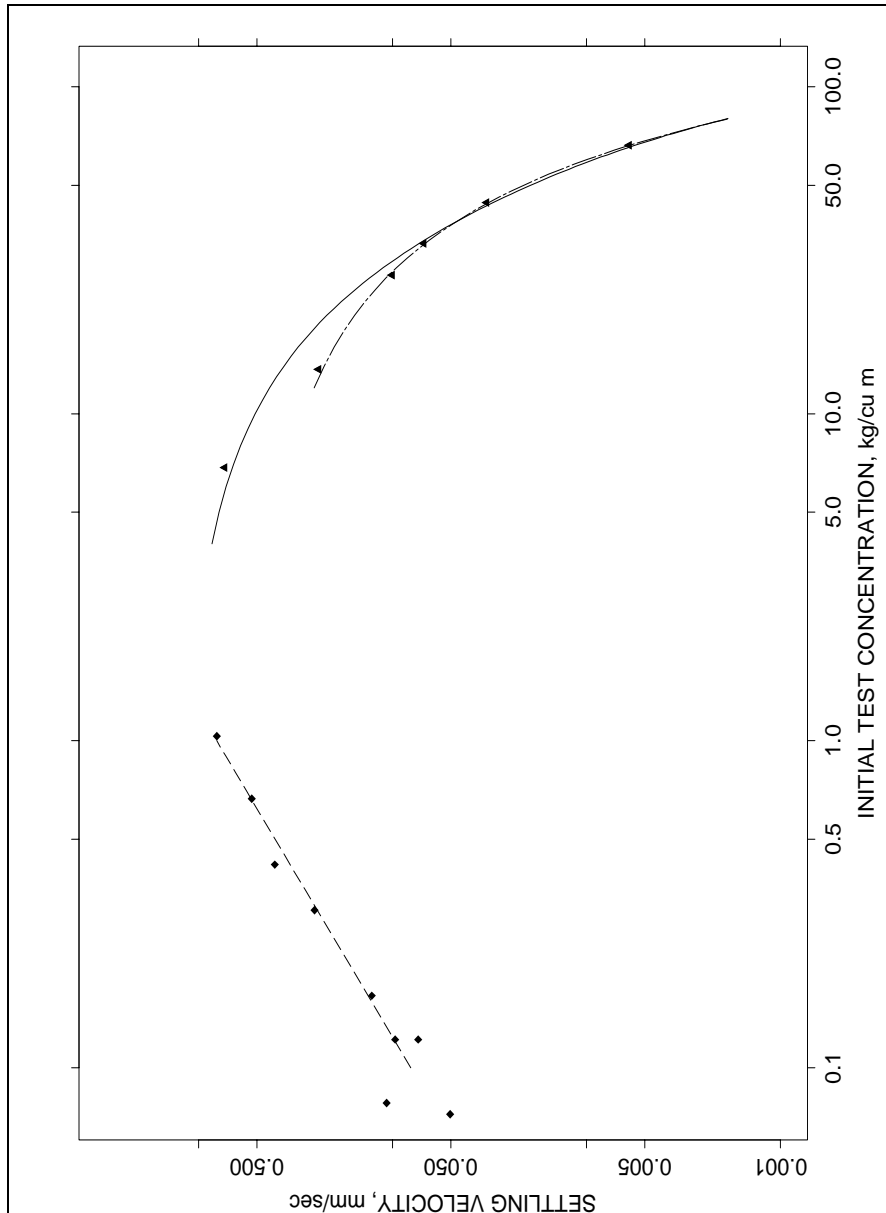


Figure 51. Hindered settling test results (right) with the (dashed) fit to the data described in the text, and low-concentration settling results (left) from Teeter et al. (2001a)

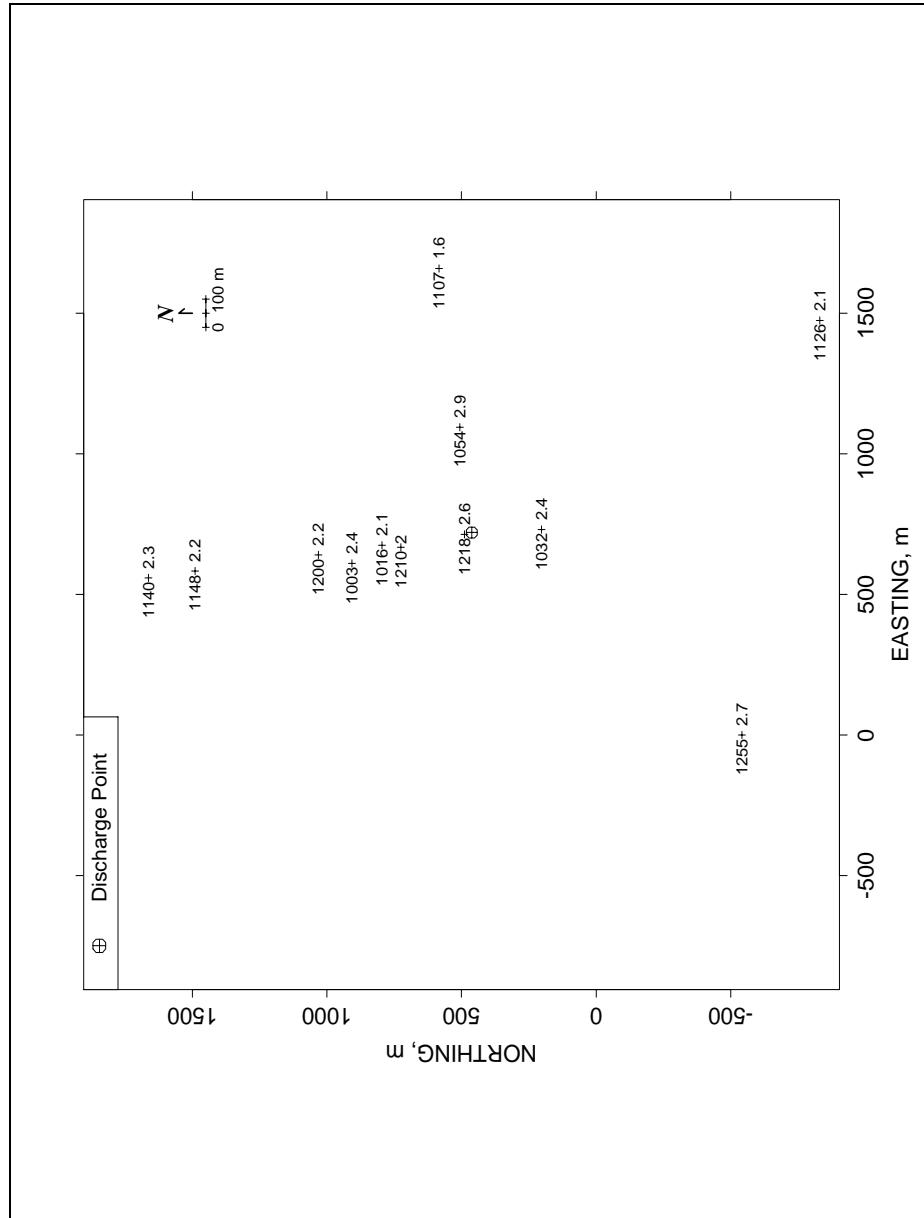


Figure 52. Times/depths (CST/m) for stations taken 10 February 2000

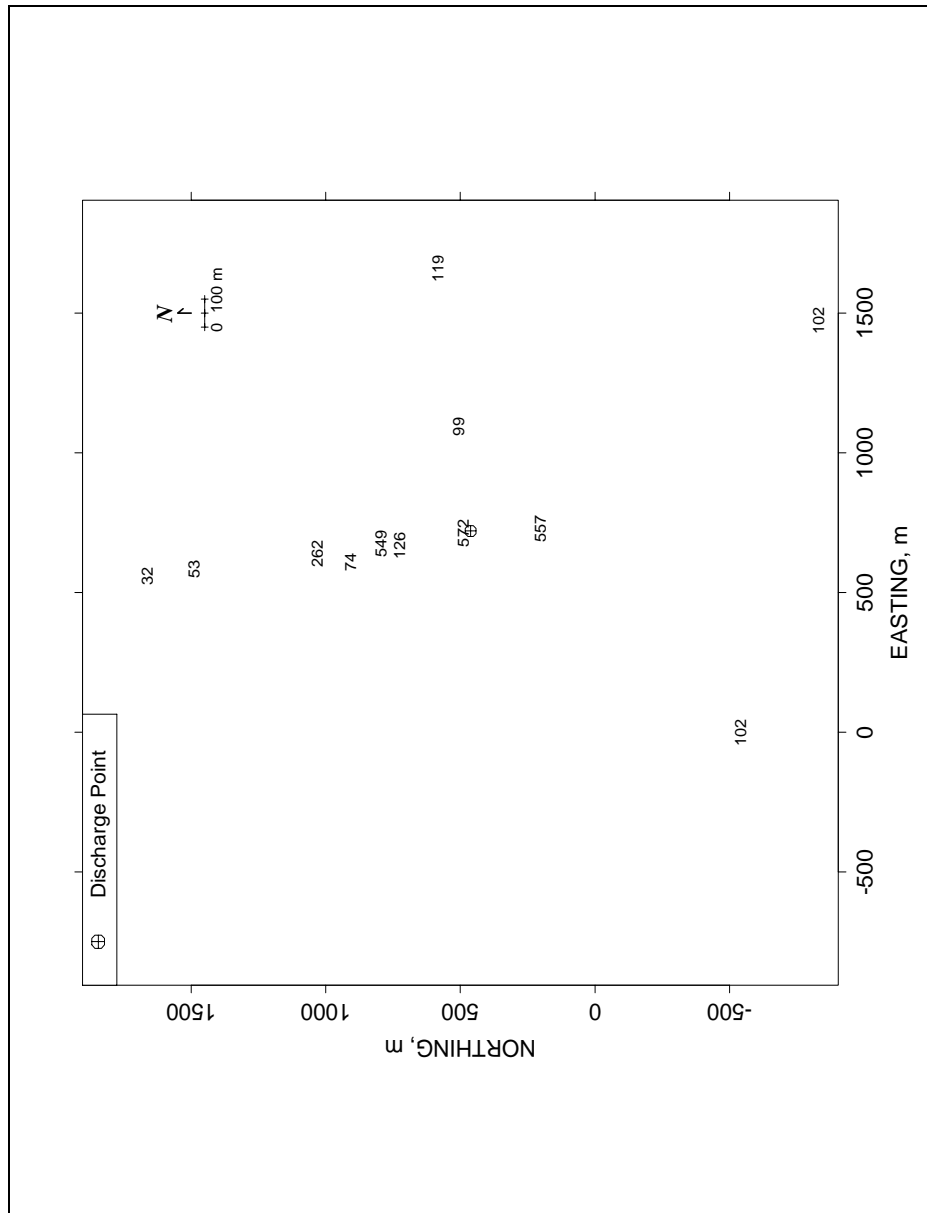


Figure 53. Depth-averaged TSM (mg/l) collected 10 February 2000

A photograph taken from 1,900-m altitude above the dredging operation at 1019 CST is shown in Figure 54. The pipeline length was about 450 m and discharged to the east of the channel. Ambient and dredged-material plumes at both the dredging and disposal sites are shown in the photograph. The aerial photograph shows the area directly south of the discharge to be the heaviest visible plume. A plume emanating directly from the discharge had a blue coloration, while other plume areas were milky. A band of less turbid water was evident near the channel and samples at 1140 and 1148 CST indicated 30 to 50 mg/l in this areas. Stations taken at 1003, 1107, 1126, and 1255 CST had what was apparently background for the area east of the channel ranging from about 75 to 125 mg/l. Depth-average TSM values of 549, 557 and 572 mg/l were obtained near and down-drift within about 660 m of the discharge. One station (1200 CST) taken upstream of the discharge had 262 mg/l TSM, possibly as the result of local resuspension.

February 16. Winds were from the south. Waves were 0.30 m or less. Currents were weak and moved toward the north (≈ 2 cm/sec). The pipeline discharge was located at coordinates $26^{\circ} 44.9752'$ N and $97^{\circ} 27.3349'$ W, about 3.3 km south of the entrance to the Land Cut, at PA 213. See Figure 49. The discharge was about horizontal onto a dredged-material mound with the pipe resting on the bottom in about 0.3-m water depth to the east of the channel. Dredging records indicated that the previous discharge location was 360 m north in PA 213. Discharge started there at about 2200 CST on 15 February; the discharge that was sampled began at about 0800 CST on 16 February. During the sampling period, 12,000 to 15,000 m³ of dredged material was discharged at these two sites.

Station times and depths are shown in Figure 55. The origin for the local coordinate system is at state plane 120,000 m N and 713,000 m E (NAD27, Texas South). A turbulent surface flow formed in the vicinity of the discharge jet and extended into deeper water. A photograph of the surface jet and flow is shown in Figure 56. A plunge line could be clearly seen in the field at a water depth of about 1 m, and an underflow moved toward the deeper water to the east-southeast. Samples taken at 0915 CST were within the turbulent surface flow, and two field measurements and two pump samples indicated that the turbulent surface flow averaged 17 dry-kg/m³.

Fluid mud formed a sharp interface with the ambient suspension, and its thickness was easily measured through the clear core tube. Fluid-mud profiles are presented in Figure 57. Because of concerns about settling effects and time constraints, few samples near the upper underflow interface were made. The fluid-mud layer was highly stratified in the vertical. Gradients indicated that concentrations at the upper interface were low. Several measurements indicated minimum underflow concentrations of 3 to 5 dry-kg/m³. However, the upper surface of the underflow was a distinct, sharp interface, indicating a concentration jump associated with the maximum flux of suspended material (Teeter 1986). Concentrations in the underflow were therefore above the concentration at which the maximum settling flux occurred. The maximum settling flux apparently occurred between the settling flux at 6.8 dry-kg/m³ (0.0051 kg/m²/sec) determined in the hindered settling tests and the previous

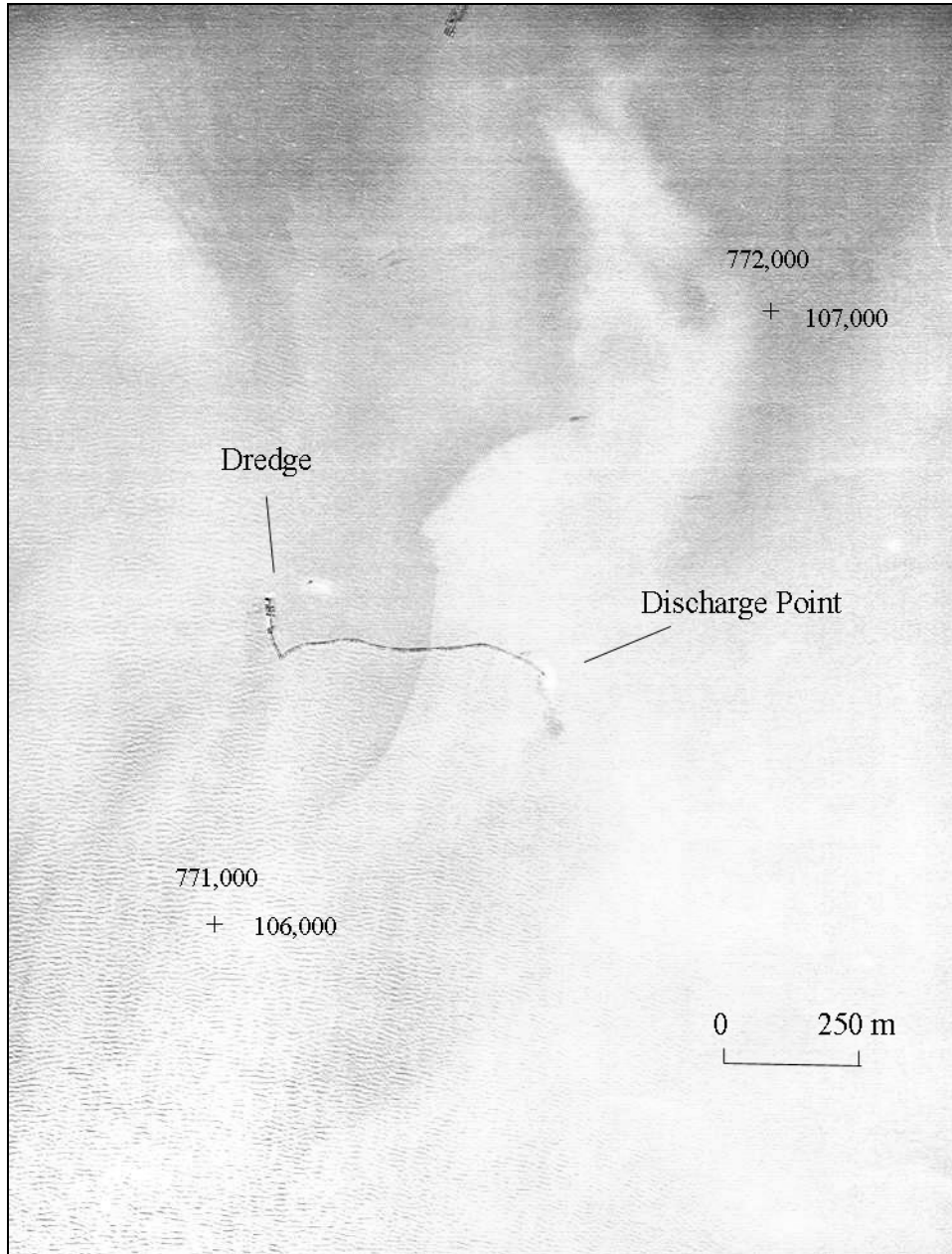


Figure 54. Overflight photo of the dredging and disposal operation taken 1019 CST 10 February 2000 (coordinates are state plane NAD27, Texas South, in meters)

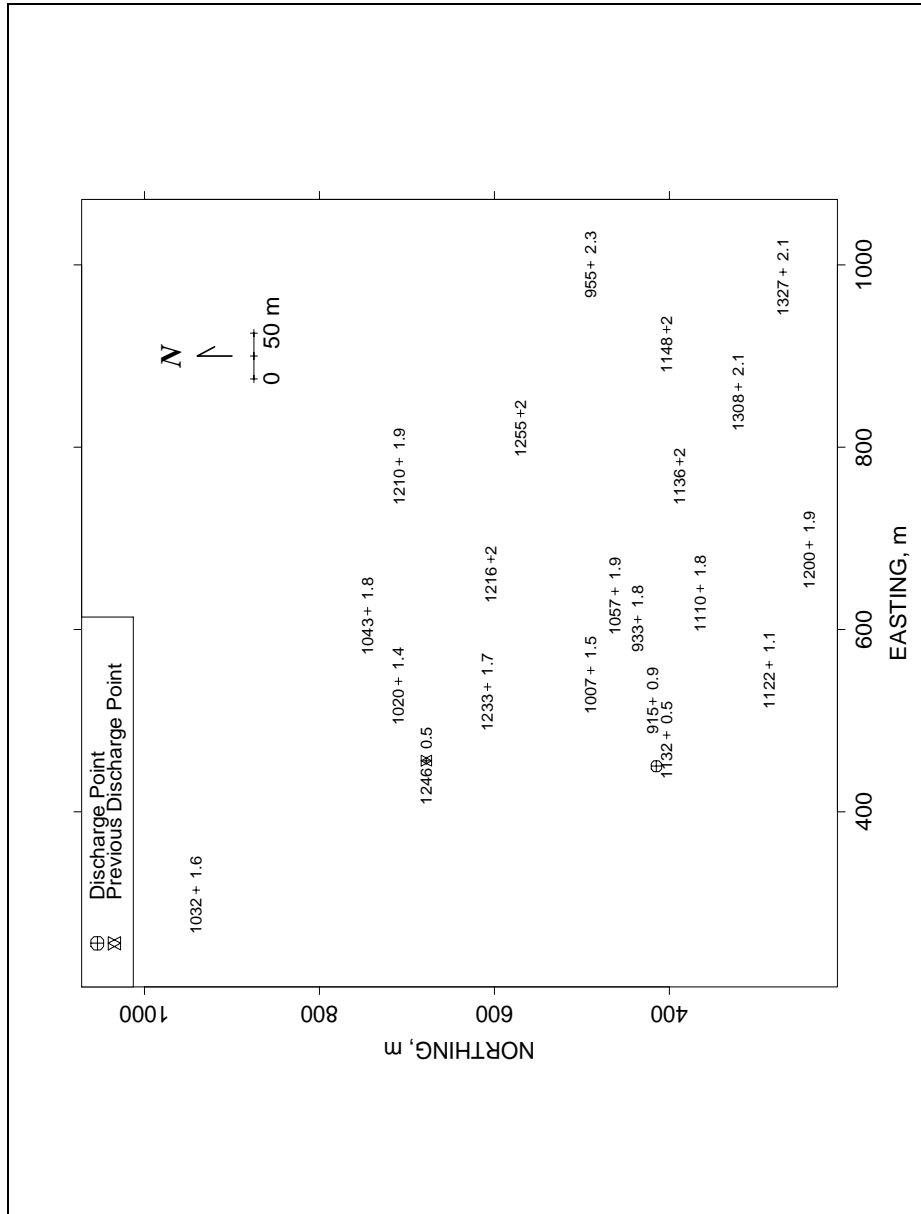


Figure 55. Times/depths (CST/m) for stations taken 16 February 2000

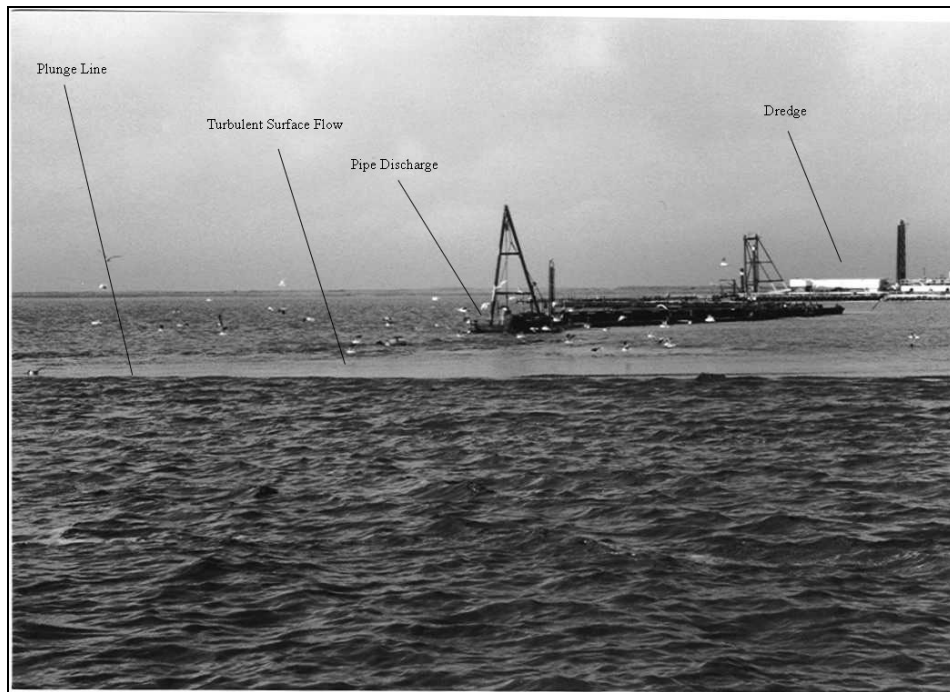


Figure 56. Photo of a pipeline discharge into about 0.5 m water depth and the resulting turbulent surface flow

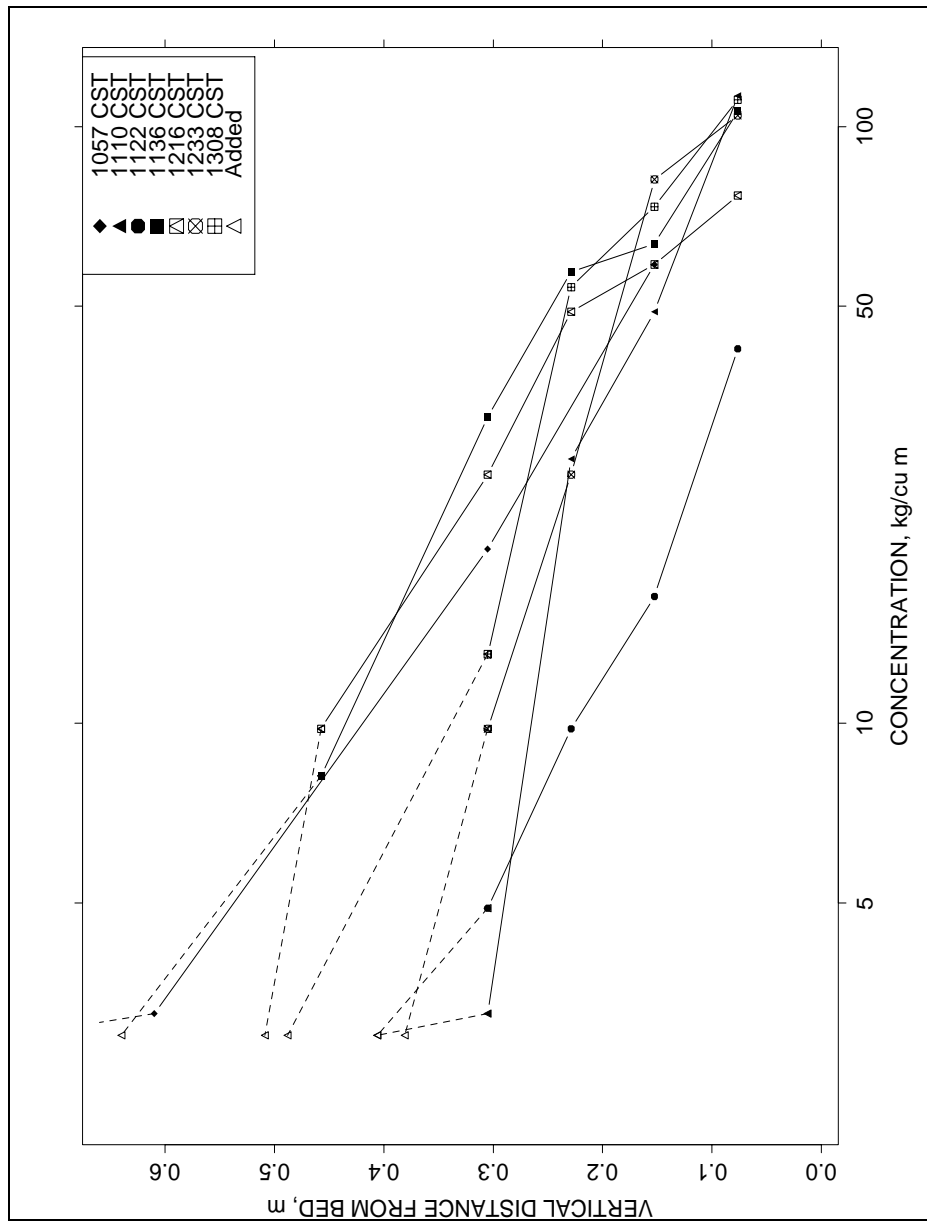


Figure 57. Vertical fluid mud profiles taken 16 February 2000

1 dry-kg/m³ low-concentration test (0.0006 kg/m²/sec). Thus, 3 dry-kg/m³ was estimated to be the minimum or underflow interface concentration. Points were added to profiles as shown in Figure 57 at the measured interface locations and the assumed 3 dry-kg/m³.

Fluid-mud layers consisted of underflow and deposit, as interpreted by the following information. Near the top of the fluid-mud layers, concentrations increased exponentially with depth and in approximately straight lines when plotted on semi-log axes as in Figure 57. This distribution would be expected for a turbulent flow with a particle Peclet number ($Pe = W_s h / K_z$ where h is the underflow thickness and K_z is the layer-average turbulent diffusivity) greater than about one (Teeter 1986). Another steeper gradient was evident below many of these exponential layers, and, taking all measurements together, the statistical distribution of fluid-mud concentrations had an inflection at about 50 dry-kg/m³. Previous laboratory experiments on sediment from nearby Corpus Christi Bay (76 percent clay and 21 percent silt) indicated that the mean concentration of newly-deposited material was 46 dry-kg/m³ (Teeter 1986). Therefore, the lower portion of these fluid-mud layers was interpreted as deposit from the underflow, while the upper layer, with concentrations of about 3 to 48 dry-kg/m³, was interpreted as the underflow. Normalized underflow concentration profiles were very similar, as can be seen in Figure 58, and their exponential shapes suggest some degree of vertical mixing, consistent with a flow with some turbulence.

All measured fluid-mud thicknesses and a rough interpretation of the underflow footprint extent are shown in Figure 59. The 0915 CST samples were assigned 0.0 fluid-mud thickness in this figure because they were located within the turbulent surface flow and therefore not technically within the underflow. It appeared that the underflow footprint formed by the discharge ongoing during sampling overlapped that formed at the previous discharge location. Underflow mean concentrations C , thickness h , and deposit thickness $delbed$ were calculated on the basis of a 50-point interpolation over the fluid-mud profiles as shown in Figure 60 for these stations, along with the water column depth above the underflow (H_o).

Surface TSM levels (mean = 258 mg/l, 95 percent confidence interval 114 to 402 mg/l, n = 17) and mid-depth levels (mean = 262 mg/l, 95 percent confidence interval -205 to 728 mg/l, n = 8) were equivalent again this day. A plot of depth-mean TSM values is shown in Figure 61, along with an interpreted underflow footprint extent. As can be seen, the highest suspended concentrations occurred over the underflow, whether upstream or downstream from the discharge point. The implication is that wind-waves were acting to entrain material from the active underflow and from the previous underflow into the water column. Since water-column advection was minimal, the highest concentration of the resulting TSM plume did not appear to extend much beyond the footprint extent (and vice versa), and suspended sediment concentrations decreased rapidly beyond the footprint area.

Comparisons between field measurements and laboratory densities indicated that many field samples had sampling errors and were biased toward lower density. These samples took much longer to obtain than the field density

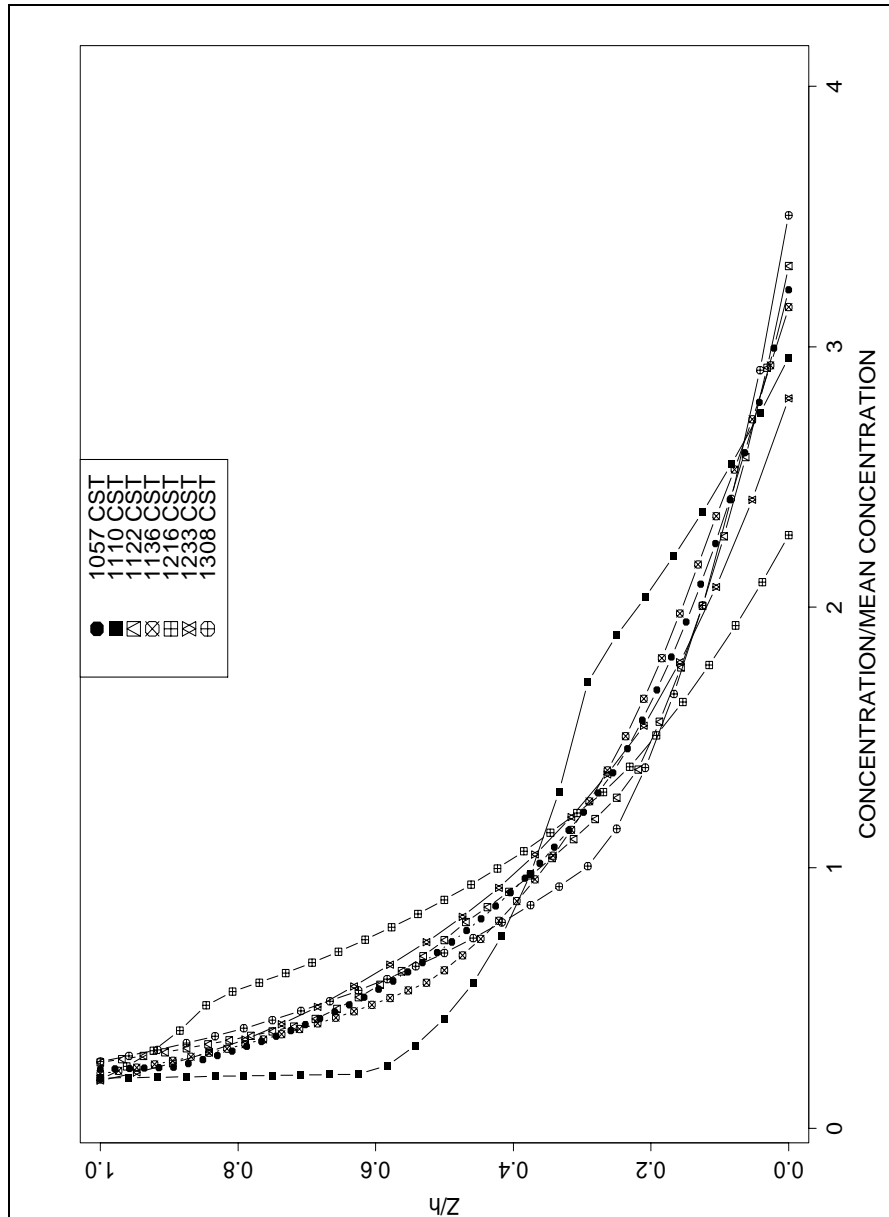


Figure 58. Interpreted and interpolated underflow profiles normalized by underflow thicknesses and mean concentrations

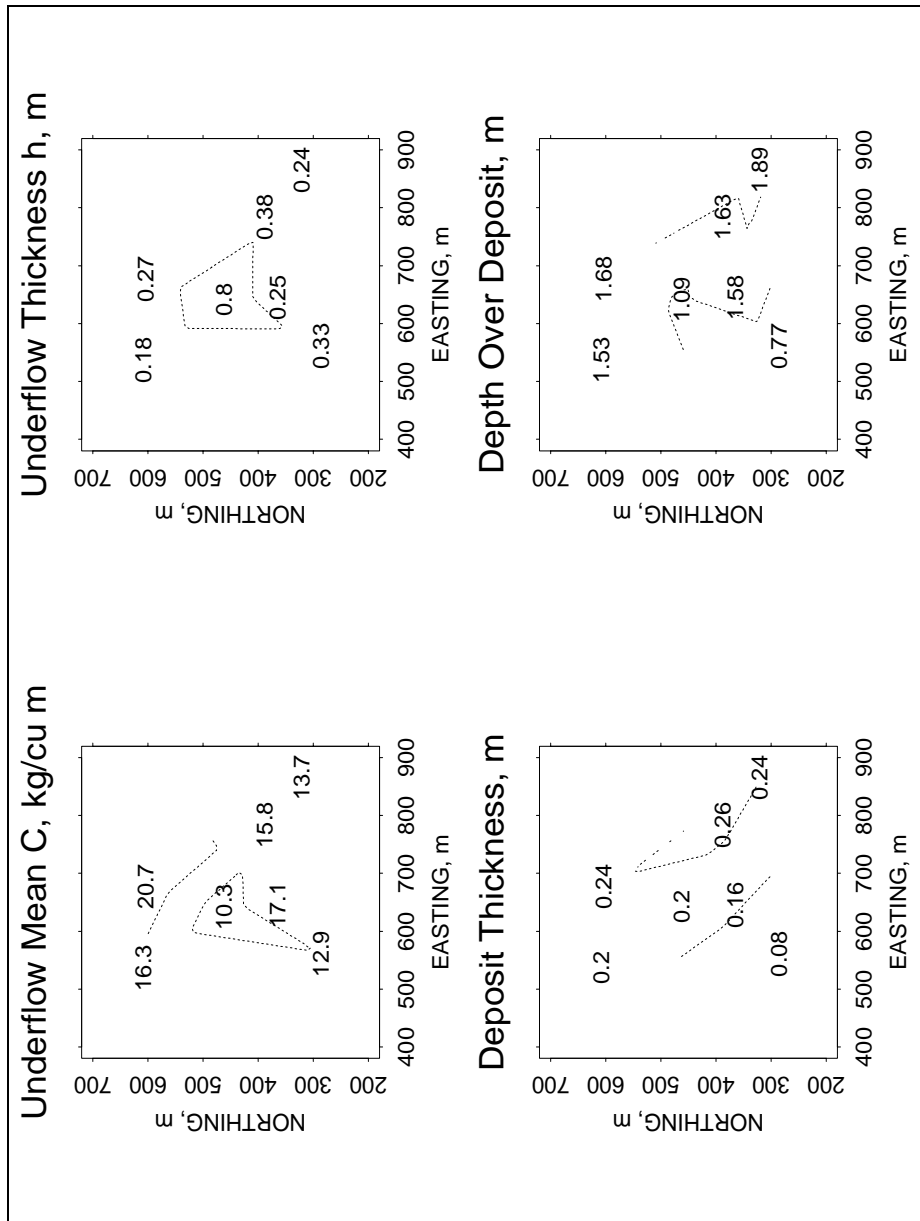


Figure 59. Fluid-mud thicknesses collected 16 February 2000

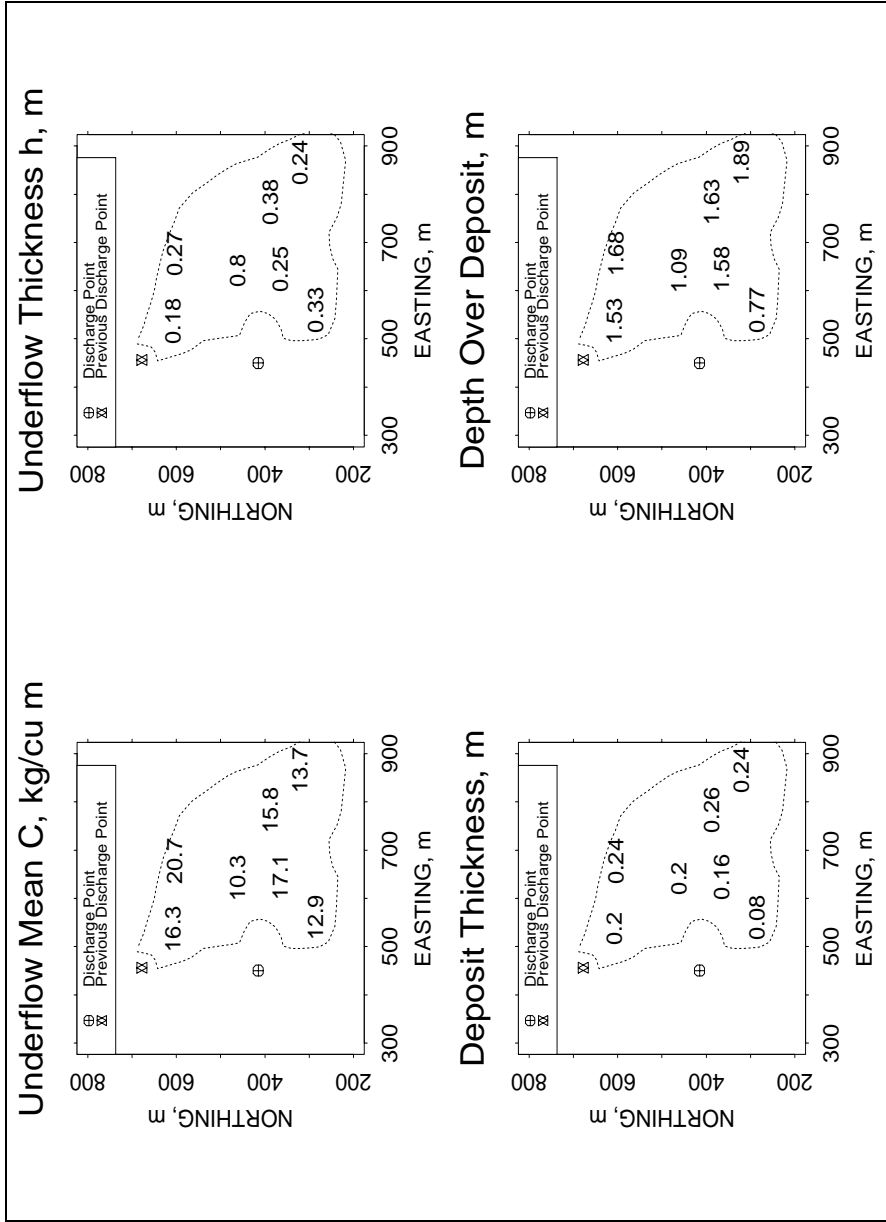


Figure 60. Interpolated underflow mean concentrations, thicknesses, deposit thickness, and water-column depth over the underflow for mud profile stations 16 February 2000

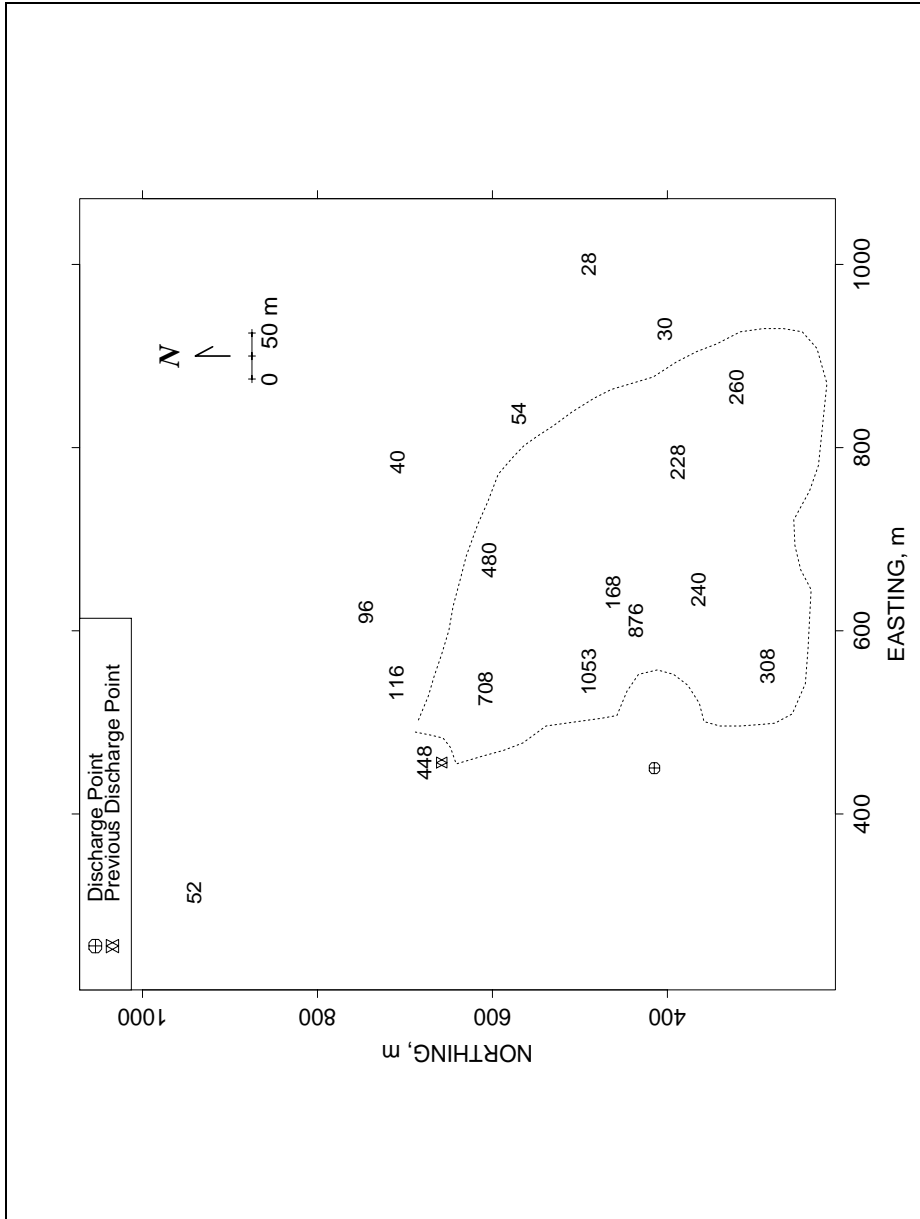


Figure 61. Depth-averaged TSM (mg/l) collected 16 February 2000

measurements did, and settling may have caused the bias. Results from the field densitometer and pycnometers agreed well on samples tested in the laboratory. Therefore, density results from samples were not included in previous figures or reported below. Laboratory analyses of particle-size characteristics on fluid-mud point samples are summarized in Table 32. In that table, H is water depth to the original bed, z_i is the distance up from the bottom, and D50 is the median dispersed grain diameter. Some variable definitions are shown in Figure 62.

Table 32 Summary of Fluid-Mud Sediment Characteristics from Near Pipeline Discharge					
Time, CST	H , m	z_i , m	D50, μm	% < 4 μm	% < 16 μm
915	0.9	0.6	4.4	47	84
915	0.9	0-0.15	5.1	43	79
933	1.8	0-0.15	5.1	43	78
1007	1.5	0.15	4.2	49	86
1007	1.5	0-0.15	4.1	50	85
1057	1.9	0.3	3.9	50	87
1057	1.9	0-0.15	4.3	49	84
1110	1.8	0-0.15	4.4	47	85
1122	1.1	0-0.15	4.2	49	86
1136	2	0-0.15	4.1	49	86
1216	2	0-0.15	4.1	50	86
1233	1.7	0-0.15	4	50	88
1308	2.1	0-0.15	4.2	50	86

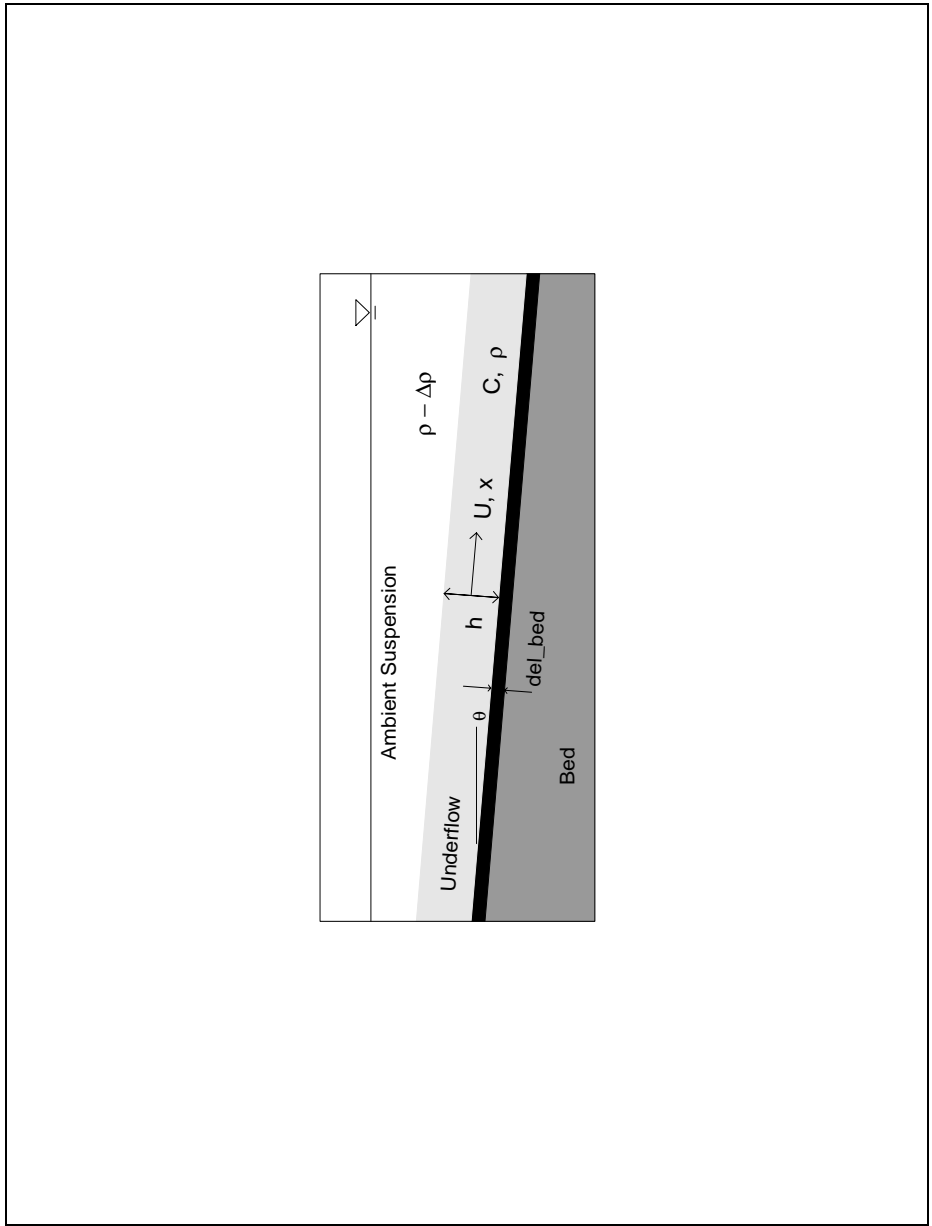


Figure 62. Definitions for some variables

Underflow Spreading Processes

The spreading of a dense underflow depends on its initial momentum and bottom slope, as well as flow rate, underflow thickness, bottom friction (dependent on flow regime), entrainment of water mass and momentum from the overlying water column (dependent on current regime), and deposition. To better understand the spreading of the fluid-mud underflow, a mathematical description of underflow processes was recently developed for dredged material pipeline discharges based on the data reported here (see Teeter 2001; Teeter 2002). Unfortunately, there are no analytic solutions for the case of a particle-driven gravity flow which is entraining and depositing material, so a numerical solution was developed. The predictive capability of the model is dependent on rather extensive site-specific field information. Important factors include sediment composition, settling and rheological characteristics, bed topography, ambient currents, winds, and waves.

The flow regime of the underflow is described by Richardson and Reynolds numbers. The bulk Richardson number for the flow is

$$Ri = \frac{g \Delta \rho h \cos \theta}{\rho U^2} \quad (39)$$

where g is the acceleration of gravity, $\Delta \rho$ is the density difference between the underflow and the water column, h is the underflow thickness, θ is the bed slope, ρ is the underflow density, and U is the underflow velocity. The underflow begins with a Ri of about 1 which is the transition between super- and sub-critical flow. The Reynolds number depends on flow properties of the slurry. These properties are very different from water and include both viscosity μ and a yield stress τ_y , both strongly dependent on sediment concentration and clay content. The Reynolds number determines the transition from laminar to turbulent and hence is important to entrainment, frictional characteristics, and deposition.

Data on the rheological properties of natural muds in the concentration range reported in the last section are very scarce. Some data for low-concentration fluid muds from Gulfport Harbor, Mississippi, are presented in Figure 63. Those data were developed from shear stress sweeps, starting below the yield stress, with a Carri-Med controlled-stress rheometer and specially collected samples (Teeter 1993).

Measurements of yield stress were made on three channel sediment samples from Laguna Madre 6 km north of Port Isabel. Samples represent the top 7.5-cm of sediment cores and all had solids contents of about 400 dry-kg/m³. Yield stresses for these samples, and for other natural muds including Gulfport, are shown in Figure 64. These data indicate that yield stress values of Laguna Madre mud are not as great as for some other natural muds at solids contents of 400 dry-kg/m³.

Entrainment into the Water Column

Entrainment of material from the underflow into the water column, the reverse of that entrainment described earlier, was implied by observed plumes of

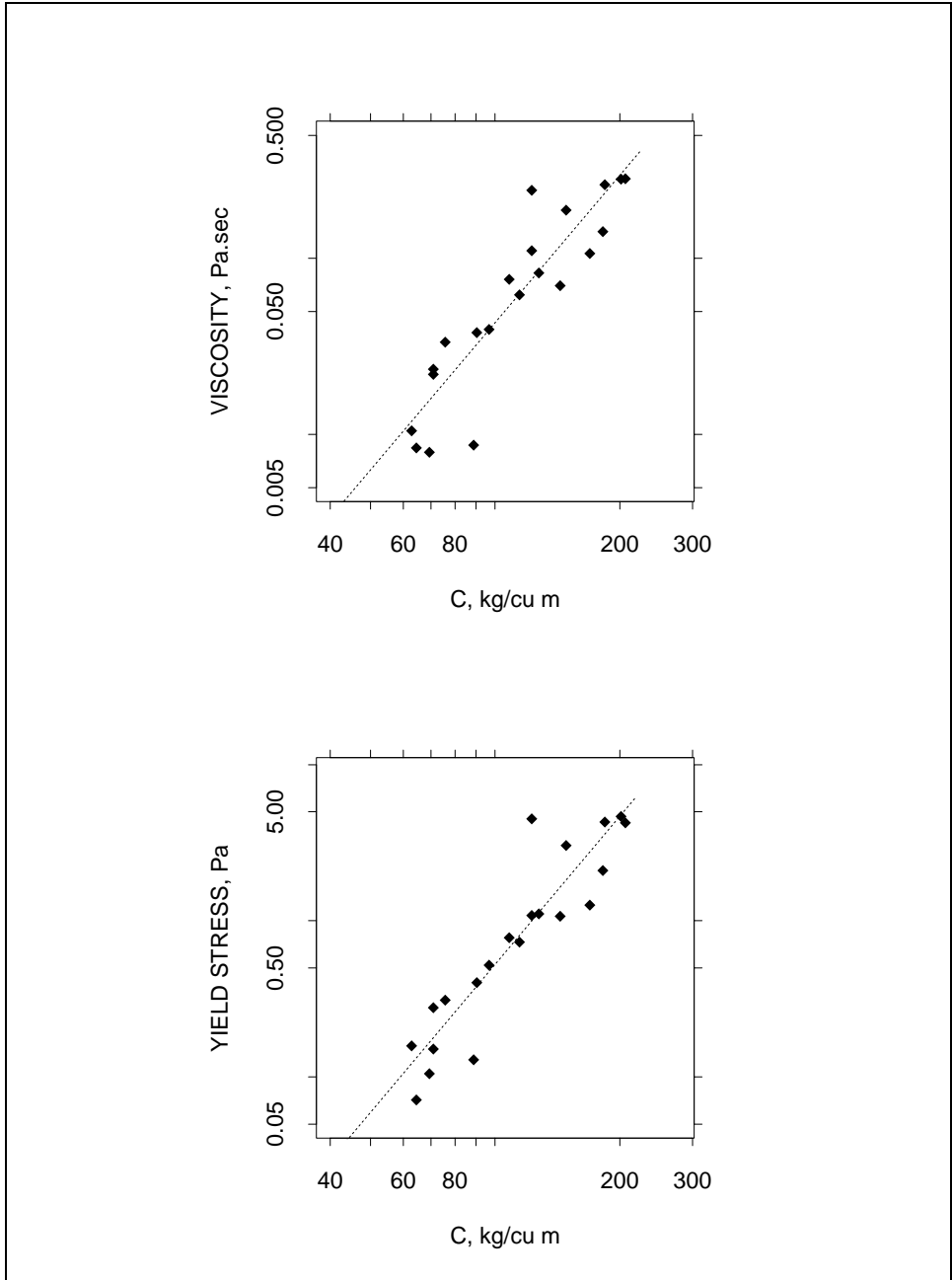


Figure 63. Viscosity at 50 sec^{-1} shear rate and yield stress for fluid mud from Gulfport Harbor, Mississippi

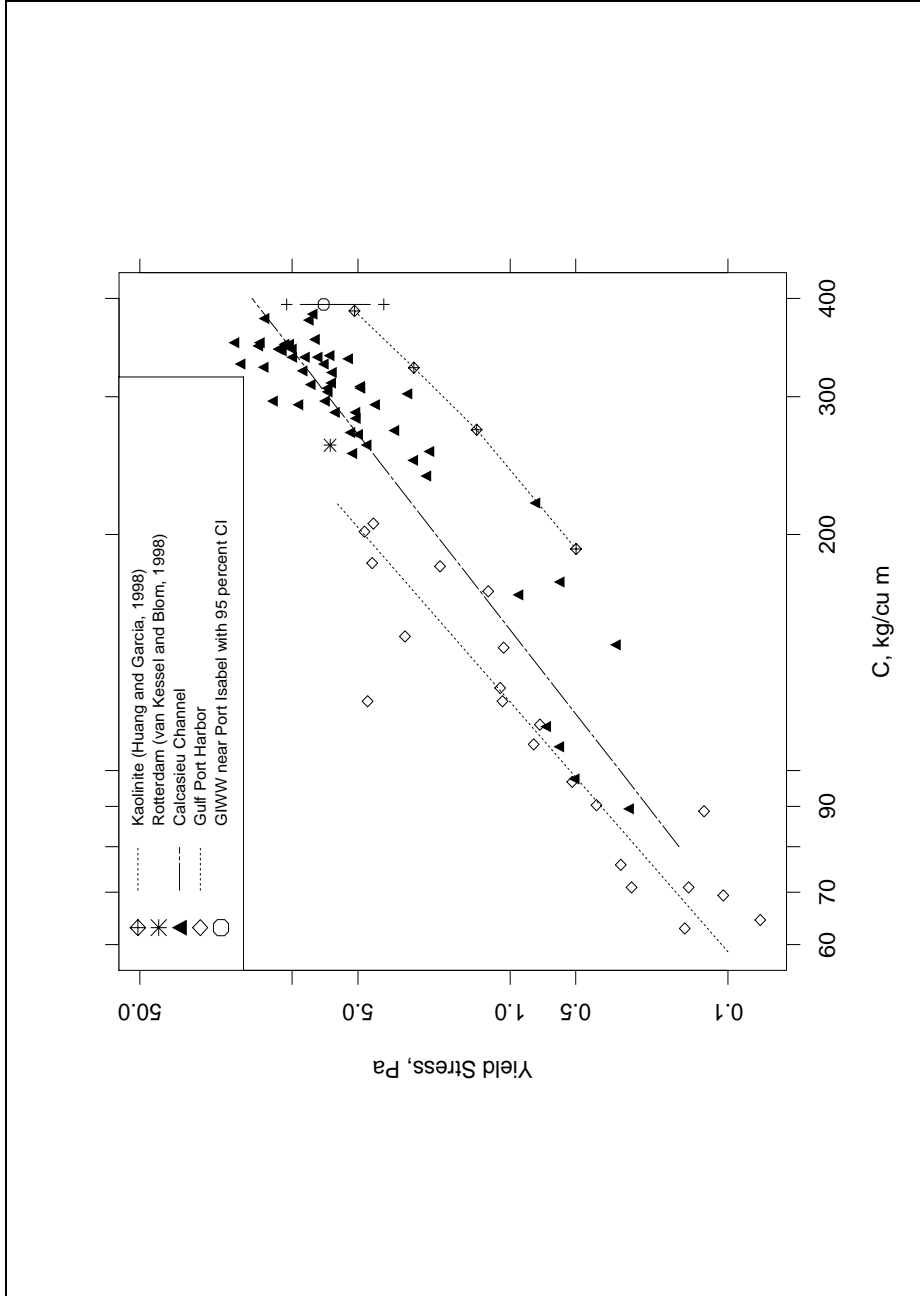


Figure 64. Yield stress for Laguna Madre GIWW sediments and other muds

suspended sediments associated with the location of the underflow footprint. In a deeper estuarine field situation, no such plume was observed by Thevenot et al. (1992). Though currents were weak at the Laguna Madre site, winds were relatively strong. The entrainment process depends on the local momentum balance, turbulence at the underflow interface, and the magnitude of density differences. Data collected on 16 February at Laguna Madre were used to make an evaluation of the entrainment process in this section.

Details of the underflow interface with the water column are important to this entrainment process. Either the density step between the water column and the underflow, or, if no such step exists, the gradient at the top of the underflow is used to scale a Richardson number (Turner 1986). As discussed earlier, the underflow was observed to be highly stratified but with a sharp density jump between its upper surface and the overlying water column. Therefore, the magnitude of the jump, along with the depth of the water column above the underflow (H_o), was used to scale a Richardson number. The magnitude of that jump was much smaller than the overall mean density difference between the two layers.

The major momentum input was from the wind. Wind data from a station at Rincon maintained by Texas A&M University, Conrad Blucher Institute, indicated that mean wind speeds at 10-m height (U_a) were 12.0 m/sec for 1000 to 1200 CST on 10 February, and were 7.6 m/sec for 0900 to 1300 CST on 16 February (standard deviations for both time periods were about 1 m/sec). An approximate location for Rincon is given in Figure 49.

Hydrodynamic forcing was assumed to equal the wind stress, some of which goes into waves and some of which goes into currents. Wind-waves in Laguna Madre tend to be at a fully-developed, depth-limited state such that dissipation is nearly equal to the momentum input (see Chapter 2). Aalderink et al. (1985) compared two models which used wind stress directly with two models which used near-bed wave orbital shear stress, and found that the models which used wind stress directly were better able to match observed TSM. The in-water friction velocity was estimated from

$$u_* = (\rho_a C_d / \rho_o)^{1/2} U_a \quad (40)$$

where ρ_a and ρ_o are the atmospheric and water column densities and C_d is the shallow-water atmospheric drag coefficient taken as a function of depth and wind speed (see Chapter 2). The average value for u_* on 16 February was about 0.0095 m/sec.

At high interfacial Richardson numbers (Ri_*), dimensionless entrainment (E) is the result of perturbations in the interface between the turbulent water column and the underflow. (Also assuming that the molecular Peclet number $= u_l l_l / \nu$ is greater than 200 where u_l and l_l are the turbulent velocity and length scales, and ν is molecular diffusivity.) Under conditions of turbulence without mean-flow, the laboratory experiments of Long (1975), and E and Hopfinger (1986) confirmed the $-3/2$ power law described by Linden (1973) that

$$E = \frac{u_e}{u_*} = K Ri_*^{-3/2} \quad (41)$$

where u_e is the entrainment velocity or the downward velocity of the interface, K is a constant, and the interfacial Richardson number is defined slightly differently from Ri as

$$Ri_* = \frac{g \Delta \rho H_o}{\bar{\rho} u_*^2} \quad (42)$$

where the density step across the interface $\Delta \rho = \rho - \bar{\rho}$, $\bar{\rho}$ is the average density of the layers, and H_o is the depth of the water column above the underflow. The scales for $\Delta \rho$ and length can be chosen differently in different entrainment systems. Here, although the underflow is stratified, the mechanism causing that stratification involves settling and not diffusion across an interface. Thicknesses of density interfaces are typically about 6 percent of the depth of mixed layers, much thinner than the stratified underflow layers observed here. Values of Ri_* are large, and interfacial perturbations are probably intermittent, consisting of vortex rebounding. Thus, $\Delta \rho$ and H_o were scaled by the overall density step and the depth of the water column.

Entrainment and deposition to the underflow by settling are assumed to be simultaneous processes in this case. Teeter (1994) reviewed laboratory entrainment experiments involving suspensions and found them to be consistent with an assumption of simultaneous entrainment and settling. Thus at a depth-averaged water-column point over an underflow

$$H_o \frac{dC_o}{dt} = F_e - F_s \quad (43)$$

where C_o is the depth-averaged suspension concentration in the water column, t is time, and F_e and F_s are the entrainment and settling flux rates at the interface.

A further simplification can be made by assuming that C_o is constant. This assumption is justified since the water-column depth is small, and the time for settling or turbulent mixing is short compared to the time-scales for underflow spread and/or wind speed changes. Under equilibrium conditions of settling and entrainment, F_e and F_s have the same magnitude. Furthermore, the settling flux for the water suspension can be estimated by use of laboratory settling tests on Laguna Madre channel sediments described by Teeter et al. (2001a) and shown in Figure 51. These results were obtained by mixing suspensions with site water and allowing them to settle in a 10-cm-diam by 1.9-m-tall column under quiescent conditions. Nine initial concentrations were tested, and settling velocity (W_s) was found to increase linearly with initial concentration. A function describing concentration-dependent settling rate for Laguna Madre channel sediments is

$$W_s = a_1 C_o^n, \quad 0.1 < C_o < 1 \text{ kg/m} \quad (44)$$

where W_s is in m/sec, $a_1 = 0.806 \times 10^{-3}$ m/sec, and the exponent $n = 1$.

Settling flux depends on depositional probability, as did the depositional flux S described in the last section. Here, turbulence at the interface is assumed to be low and intermittent, and the depositional probability is assumed to be unity. The depositional flux depends on the near bed concentration C_b , but in this case it is assumed that $C_b/C_o \approx 1$. Therefore, $F_e = u_e C$ and $F_s = W_s C_o$; a simple model for the water column suspension concentration is

$$C_o = \left(\frac{K}{a_1} C u_* Ri_*^{-3/2} \right)^{\frac{1}{n+1}} \quad (45)$$

Equation 20 was recast to solve for the entrainment coefficient K with field data. The Laguna Madre measurements and Equation 7 indicated that $C_b/C_o = 1.07$, and column C_o values were adjusted accordingly. In-water friction-velocities were calculated with use of Equation 19 and a constant wind speed of 7.6 m/sec. Underflow concentration at the interface was assumed to be 3 dry-kg/m³. Results for K and other select parameters are presented in Table 33.

The flux Richardson number (Ri_f) was calculated for Table 33 as $(u_e/u_*) Ri_*$ (Turner 1986) and represents the ratio of turbulent kinetic energy dissipation by buoyancy flux and turbulent production. Flux Richardson numbers greater than 0.1 are associated with damping of turbulence, and the magnitudes of Ri_f obtained here indicate appreciable suppression of turbulence at the interface.

Time, CST	TSM, mg/l	H_o , m	Ri_*	$F_s \times 10^5$, kg/m ² /sec	K	Ri_f
1057	168	0.86	86	2.6	0.7	0.1
1110	240	0.26	133	5.3	2.8	0.2
1122	308	0.41	69	8.8	1.8	0.2
1136	228	0.37	128	4.8	2.4	0.2
1216	480	0.29	134	21.3	11.4	1
1233	708	0.2	124	46.3	22.1	2
1308	260	0.25	151	6.2	4	0.3

The K (and TSM) values were log-normally distributed. The median K value was 2.8 in fair agreement with the laboratory result of 3.8 reported by E and Hopfinger (1986). Based on this estimate for K , an estimate of C_o was made for 10 February with Equation 20. Assuming underflow conditions were the same as before, where $\Delta\rho/\bar{\rho} = 0.00081$, and that $H_o = 2$ m and $u_* = 0.0174$ m/sec, then the Ri_* for that day was about 52. Equation 20 predicts $C_o = 690$ mg/l or somewhat higher than the high values observed in the field (Figure 53).

Discussion

Some of the important results from the field measurements were as follows: the underflow thickness was relatively uniform and decreased rapidly near the limit of down-slope extent. The underflow had a distinct upper surface or interface with the ambient water column, but this concentration was only about 3 dry-kg/m³. Underflow layers were sediment and density stratified. Turbulence in the underflow was not sufficient to mix sediment vertically. Thick deposits formed under the underflow so shear stresses at the bottom of the underflow were apparently low. The implication of these observations was that the underflow was slow moving. An apparent absence of appreciable entrainment also indicated slow underflow movement and high Richardson numbers. The concentrations near this upper surface and layer average values were relatively uniform along the length of the underflow. This observation indicated the underflow collapsed vertically due to settling and while depositing and led to the model feature that tended to maintain underflow concentrations while deposition occurred.

For the February 2000 measurements, median fluid-mud thicknesses were 0.45 m of which the top 60 percent was interpreted as underflow and the remainder as deposit. Deposit thicknesses were measured with dual-frequency acoustics after the 1994 dredging and disposal event at PA 233 in Lower Laguna Madre (Brown and Kraus 1997). Maximum thicknesses were about 0.2 m some days after the dredging was complete. Monitoring in 1998 down-slope from the edge of PA 235 indicated that disposal there produced a mud deposit of about 0.4 m (Burd and Dunton 2000).

Laboratory-determined settling velocities were used in the description of underflow spreading and in the analysis of water column entrainment of underflow material. Laboratory measured values are probably not the same as field values, but obtaining measurements in the field is problematic. Wolanski et al. (1992) showed that very low levels of turbulence decrease W_s in the hindered settling concentration range by factors of 2 to 10. Data in Chapter 4 indicated that for low-concentration Laguna Madre suspended sediments, quiescent column tests yielded settling rates representative of disrupted flocs. Very mild turbulence produced much larger values, but shear rates greater than 2 sec⁻¹ produced settling rates not much different from quiescent values. The uncertainty in W_s affects the results of both the underflow and water column analyses, if performed in a predictive mode.

Our understanding of fluid-mud flow properties is incomplete and measurements are difficult. The existence of a yield stress may lead to an unsheared plug flow zone (Coussot 1994) in the underflow and could make Reynolds number values based on layer average properties unrepresentative of interface conditions where entrainment occurs. In the present case, the underflow layer was highly stratified, and the velocity profile was difficult to evaluate.

Rheological data on muds are relatively scarce. While varying rheological parameters over an order of magnitude from those used in the example calculation did not greatly affect model results, increases in viscous and yield

stress properties eventually caused the model underflow to “freeze” or stop abruptly and become numerically unstable. The range from laboratory clays to cohesive natural muds such as those in Figures 63 and 64 affect computed underflow Reynolds numbers, friction, flow, and ultimate extent of spreading.

Elevated water-column suspended sediment concentrations were caused by underflow entrainment into the water column by wind-wave forcing. Entrainment model coefficients were consistent with previously reported values for high Ri_* situations when used with wind-stress forcing.

The pipeline discharge underflow and the underflow deposit represent the greatest potential for local turbidity generation, if entrained into the overlying flow, since they contain the vast majority of sediment particles discharged. After some hours, the underflow completely deposits, unless resuspended into the water column. The field observations reported here, made under moderately high bed shear-stress, indicate that entrainment of underflow material can generate a turbid plume extending some hundreds of meters distance from the discharge, but not necessarily downstream from the discharge. Thus, the area of concern with respect to near-field water-column impacts of a pipeline discharge is not confined to the vicinity of discharge, but also includes the area above the underflow. In the case of the 16 February disposal, the maximum distance from the point of discharge to the edge of the high turbidity area was about 500 meters (0.3 mi).